Sensors and Actuators A 295 (2019) 503–511

Contents lists available at ScienceDirect

Sensors and Actuators A: Physical

journal homepage: www.elsevier.com/locate/sna

Colorimetric and plasmonic pressure sensors based on polyacrylamide/Au nanoparticles

Gokhan Topcu, Tugrul Guner, Ezgi Inci, Mustafa M. Demir*

Department of Materials Science and Engineering, İzmir Institute of Technology, 35430, Gülbahçe, Urla, İzmir, Turkey

ARTICLE INFO

Article history:
Received 11 March 2019
Received in revised form 6 June 2019
Accepted 17 June 2019
Available online 18 June 2019

Keywords:
Au clusters
Au nanoparticles
Disassembly
Plasmon coupling
Plasmonic shift
Polyacrylamide

ABSTRACT

Colorimetric stimuli-responsive nanomaterials have emerged as an eminent tool for sensor applications. Among this class of sensing elements, gold nanoparticle-based (Au NP) nanostructures are promising materials due to their plasmonic features. In this study, free-standing flexible polymeric films having intense optical response upon application of mechanical pressure were fabricated based on polyacrylamide (PAAm) and Au NPs. Pressure may cause plasmonic shift most probably due to the disassembly of the clusters from blue to reddish individual particles depending on the extent of pressure. Temperature, time, and extent of pressure were examined in terms of spectral change of Au particles. The sensor films depict working range up to 160 MPa, which shows minor change at elevated temperatures probably due to the stress induced crystallization of PAAm. For practical applications, a simple red-green-blue (RGB) space-based algorithm was presented for smartphone-assisted detection of applied pressure. Moreover, the PAAm/Au composite structure shows self-healing without any additive under ambient conditions even after divided into pieces.

1. Introduction

Mechanical sensors are tools that ease daily life by sensing external mechanical stimuli for instance pressure, stress, strain, impact etc. and converting them into an assessable output. Among them, pressure sensing materials are of remarkable importance for diverse future applications such as touch-on flexible displays [1], electronic skin [2,3], and soft robotics [4,5]. To date, pressure sensors are typically based on the sensing materials having force-induced changes in their piezoelectricity [6,7], capacitance [8], triboelectricity [9], and resistivity [10]. The need to develop pressure sensors that can precisely give the output in the desired manner requires the rational design of innovative devices and materials. Even though various nanomaterials such as nanowires [11], metal nanoparticles (NPs) [12], polymer nanofibers [7,10], and carbon nanotube [13] have been employed to design of futuristic pressure sensors, these nanomaterial-based pressure sensors are predominantly based on electrical properties of sensing element. Nevertheless, only limited number of studies based on pressure sensing materials giving optical response has been reported. For instance, it is stated that the chameleon-inspired nanocomposite containing a close-packed arrangement of SiO_2 NPs in polymer matrix exhibits various vivid colors upon external mechanical forces including stretching and compressing [14]. Motivated from nature, the strain responsive structural colored elastomers, which have polymeric colloidal crystal assembly in poly(ethyl acrylate) matrix is also reported [15]. On the other hand, Han et al. proposed that Au NP-poly(vinyl pyrrolidone) composites can possess color transformation under compression [16]. Therefore, the nanocomposites containing colloidal NPs have become prominent emerging materials for pressure sensor application presenting optical output.

Colloidal NPs have attracted intensive research interest not only owing to their size- and shape-dependent features but also the development of novel and unique properties through their collective effects such as interparticle coupling and structural ordering [17–19]. Hence, the controllable geometry and properties depending on the assemble behavior make them promising candidates for wide range of applications from stimuli responsive smart materials to sensors [16,20,21]. Gold nanoparticles (Au NPs) appear to be a good example for this group of materials since they have optical properties distinct from analogous atomic or bulk counterparts. Upon illumination with incident electromagnetic beam, the free electrons are confined and exhibit collective oscillation that leads to absorption of visible light. This phenomenon is termed as localized surface plasmon resonance (LSPR) [22].

* Corresponding author.
E-mail address: mdemir@iyte.edu.tr (M.M. Demir).

https://doi.org/10.1016/j.sna.2019.06.038
0924-4247/

For colorimetric sensors that give optical response according to the measurand, there are various strategies based on color change. A dramatic colorimetric change upon aggregation of Au NPs is one of the well-known systems among others [23–25]. The particles can be assembled or disassembled either by varying ionic strength or by changing pressure so that LSPR coupling-induced responsive color may switch from red to blue, or vice versa [26]. The sensing strategy based on the change of LSPR properties of Au NPs can be designed to detect the presence of external conditions, and even more, their magnitude can be estimated. This strategy allows to perform a wide variety of functions such as chemical and biochemical sensing [27–33], pH [26,34,35], pressure [16,21], temperature [36–38], and photosensing [39–41]. Furthermore, upon removal of existing stimuli, the system may relax back to the initial state. Therefore, the reversible characteristics of plasmonic nanoparticle-based colorimetric sensors offer the potential of improved specificity and long-term availability as one can use the sustained stimulus-response function in diverse precision for measurement.

Among LSPR-based sensors, mechanical sensors are promising materials, in which viscous flow of polymeric materials during deformation leads to the shift in plasmonic band via disassembly of Au NP aggregates [16,42,43]. Mechanical and chemical properties of the polymers that are used as a matrix for colorimetric pressure sensors are vital since the motion of Au NPs is either facilitated or prohibited. The former feature determines reversibility of sensor depending on the elasticity of the polymer while the latter one is responsible from the interaction of the polymer macromolecules with the Au NPs surface, which is able to enhance the disassembly rate of these nanoparticles. Polyacrylamide (PAAm) and its derivatives are appropriate to use in these type sensors due to its viscoelastic properties [44], heteroatomic structure [45,46], and biocompatibility [47].

In this study, Au NP embedded PAAm composite films were fabricated and their performance as a colorimetric pressure sensor was studied. The shift in the plasmonic signals of Au particles was recorded as a function of applied force, time, and temperature. The resulting response against external mechanical force was also associated with the morphological change of both nanoparticles and polymer matrix, i.e. disassembly of Au NPs and crystallinity of PAAm. In addition, a simple RGB space-based algorithm referring to pixels of the captured images through a digital camera was presented for the design of possible pressure measuring smart-phone application.

2. Experimental

2.1. Materials

Tetrachloroauric (III) acid trihydrate ($HAuCl_4{\cdot}3H_2O$, 99%), trisodium citrate dihydrate (≥99%), PAAm solution (50% w/v, M_w: 1.5 kg/mol), and poly(vinyl pyrrolidone) (PVP; M_w: 10 kg/mol) were purchased from Sigma-Aldrich. All chemicals were used as received without any further purification. The deionized water (18.2 MΩ•cm^{-1} at 25 °C) used in all experiments was produced by a Milli-Q Advantage water treatment system.

2.2. Methods

2.2.1. Synthesis of Au NPs

The synthesis of Au NPs was carried out via reduction of $HAuCl_4$, i.e. Turkevich method [48]. In a typical synthesis, an aqueous solution of $HAuCl_4$ (0.24 mM, 200 mL) was loaded one-necked flask and heated up to reflux with magnetic stirring. Subsequently, trisodium citrate solution (0.34 M, 1 mL) was added to system. The solution was allowed to reflux for 30 min, while its color changed from pale yellow to ruby red. Final mixture was centrifuged (6000 rpm, 1 h) and re-dispersed in 2 mL water.

2.2.2. Fabrication of pressure indicating films

PVP solution (10 μL of 1.66 mg/mL) was added to Au NP dispersion (0.5 mL) to stabilize the colloids. The PAAm solution (250 μL) was added to mixture and mixed for 5 min to obtain homogeneous blue dispersion. The mixture was then drop-casted into a mold and placed in oven for 2 h at 60 °C to allow the evaporation of water. The resulting composites were cut into small pieces with 1 mm diameter.

2.3. Characterization

The films were loaded into a hydraulic pressure apparatus (Carver Inc., Wabash, IN, USA) and constant pressures (from 40 MPa to 160 MPa) were applied at various temperatures (20, 30, and 50 °C) and times (from 1 to 5 min). The experiments were conducted at similar relative humidity conditions (55–60%). Size and surface characterization of Au NPs were carried using Dynamic Light Scattering (DLS; Malvern, Zetasizer ZS90, UK). The morphology of the particles and composites was enlightened by Scanning Electron Microscopy (SEM; Quanta 250, FEI, Hillsboro, OR, USA). Optical properties of loaded and unloaded samples were recorded in absorbance mode using USB2000+ spectrometer (Ocean Optics Inc., Dunedin, FL, USA) via a premium fiber cable. The crystallographic pattern of composites was recorded by X-ray diffraction (XRD; X'Pert Pro, Philips, Eindhoven, the Netherlands). The photographs of the films were taken with cell phone camera (Apple, Iphone 7, CA, USA).

3. Results and discussion

Au NPs were obtained by reduction of $HAuCl_4$ salts. The particles intrinsically have negative surface charge; however, upon incorporation of PVP, the overall charge gets zero and they show neutral character (Fig. S1). PVP acts as surfactant for the particles and sterically-stabilizes the individual particles, as a result prevents aggregation. The dispersion containing individual particles has deep red color. When PAAm is introduced into the system, pH of the dispersion changes from 6.8 to 5.9. Since there is only trace amount of PVP (16.6 μg in entire volume) incorporated to the mixture, citrate molecules still exist onto Au NP surface. Therefore, citrate molecules are protonated with decreasing pH, which leads to a reduction of stability, thus aggregation of the particles. Note that the amount of PVP was optimized according to the level of aggregation and an excess amount of PVP can completely stabilize the particles that hinders the change in color. Fig. 1a shows photographic image of the Au NP containing dispersions. The left image presents PVP-stabilized individual particles appearing in red. On the other hand, the right one illustrates saturated blue appearance of the particles in aggregated form. The UV-VIS absorption spectra of the particles are given in Fig. 1b. The spectrum of the individual particles has absorption maxima nearly at 520 nm; however, the aggregates of the particles present broad signal giving peak at 630 nm. The spectrum has a shoulder at 520 nm exactly at the signal of individual particles. Since both signals appear in the blue dispersion, one can propose that both individual particles and aggregates coexist together in the blue dispersion. These two signals in UV-VIS spectra appear most probably due to LSPR and plasmon coupling, respectively. The broadening of the absorption can be attributed to the clustering and/or chain structure of the Au NPs in the dispersion. The spectroscopic results agree with the ones reported in literature [49]. The diameter of the particles was measured by DLS and the

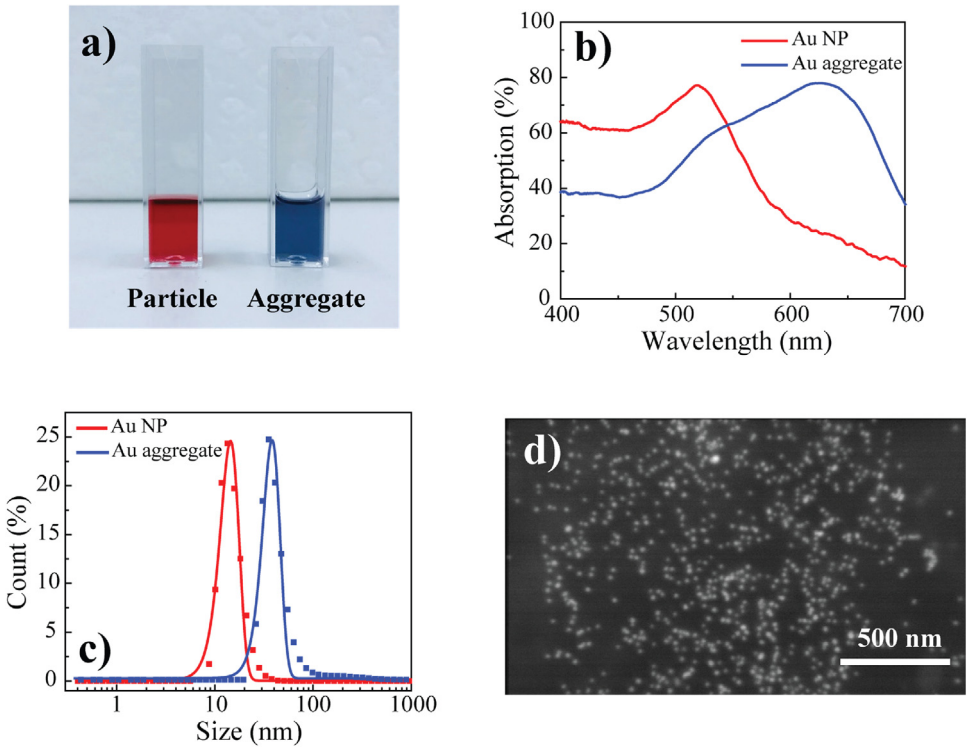

Fig. 1. (a) Photographic images of Au dispersion appearing in red (individual nanoparticles) and blue color (aggregates), (b) absorption spectra, and (c) size distribution of as-synthesized individual Au NP and aggregate dispersions. (d) SEM image of the Au NPs.

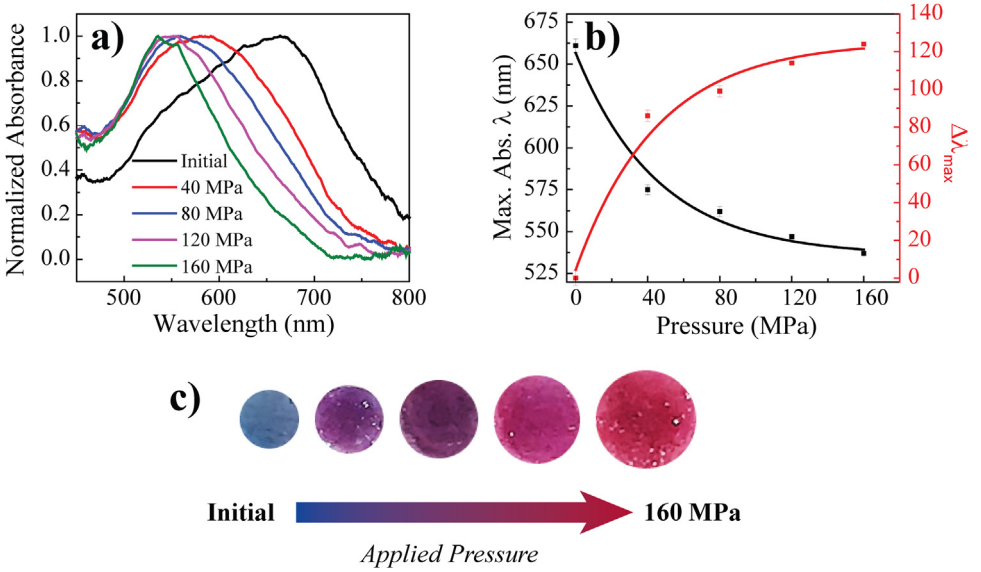

Fig. 2. (a) Absorption spectra of the films under various magnitudes of pressure, (b) corresponding maximum absorption wavelength (λ_{max}) and its change ($\Delta\lambda_{max}$) with respect to pressure, and (c) appearance of the films employed under various pressures.

results are presented in Fig. 1c. The size range is scanned from several nm to 1 μm. The diameter of individual particles is 13.5 nm and this result is consistent with the size of individual particles seen in the microscopy image (Fig. 1d). On the other hand, the size of the Au aggregates in blue dispersion is 45 nm with a uniform Gaussian distribution. The size distribution of this dispersion obtained by scattering only shows single signal in contrast to spectrometric characterization. Light scattering measurement is based on the change of the scattering profile of particle domain population in the system. Since they are in Brownian motion, the scattering profile varies depending on the size of the particles. Therefore, the existence of the individual particles in bluish mixture can be detected by spectroscopy; however, they cannot be observed in scattering profiles due to their low numbers in the particle population.

The evaporation of water induces aggregation of the particles so that the dispersion containing Au NP aggregates shows deep blue appearance after drying. These films were cut into small pieces to perform compression tests between 40 and 160 MPa. The initial pressure applied on the composite film was calculated by dividing the force by the initial area. The application of a high pressure onto the composite film for 2 min caused a clear change in color from blue to ruby red due to pressure-induced disassembly of Au NP

clusters. The change in color of the films with respect to the applied pressure is given in Fig. 2 in terms of absorption spectra and their corresponding photographs. By means of the increase in pressure, the peak of the absorbance gradually shifts from 660 to 538 nm. Compared to the particle-water dispersion (Fig. 1b), the absorption peak position exhibits a remarkable difference in the solid film state. For the initial state of film, peak position experiences 30 nm red shift. This may arise due to the evaporation-induced aggregation. On the other hand, the difference between individual Au NP dispersion and the compressed red film shows that complete disassembly may not be obtained, even if the most of the aggregates are separated after applying strong pressure. In Fig. 2b, coupling signal peak positions at various applied pressure are plotted and fitted by using exponential curve fitting. Since the more deformation causes a larger displacement for the Au NPs due to growing inter-particle distance, the extent of the shift in the coupling signal, namely change in color, increases at higher pressure (Fig. 2c). It has been established that the inter-particle distance above 10 nm, plasmons cannot couple with the surface of neighboring particle [19,50]. A morphological investigation to figure out the dispersion of the particles over PAAm volume is performed by electron microscopy. SEM images of the initial and deformed samples are demonstrated in Fig. 3. The particles appear in large clusters with a diameter of 100 nm. The aggregates in the initial state seem to be separated into individual particles as a result of deformation. The cluster is disintegrated/disassembled into individual particles by pressure.

The change in color at constant pressure with respect to time was examined studying the viscoelastic properties of PAAm. In general, Kelvin-Voigt Model allows examining the deformation of the polymer under sufficient shear stress for viscoelastic solids (**Eq. 1**) (otherwise it follows Hooke's Law under lower shear stress). The deformation is proportional with change in time under constant shear stress;

$$\varepsilon(t_0) = \int_0^{t_0} \frac{\sigma(t_0)}{\eta} dt \quad (1)$$

where ε is deformation, σ is applied stress, t is time, and η is viscosity. Fig. 4a shows absorption spectra of the film at constant pressure (40 MPa) for various time periods (t = 0, 1, 2, 3, and 5 min). A clear blue shift of the absorption maxima from 575 to 552 nm is observed as the pressure time is extended from 2 to 5 min, i.e. Au NP clusters can find more time to be separated into individual particles. Similar trend of the spectral shift was observed when the magnitude of the applied pressure is varied. The maximum wavelength (λ_{max}) of the absorption versus duration of time of the applied pressure is given in Fig. 4b. For each pressure scale, λ_{max} gradually decreases in time and saturates at approximately 538 nm. Not surprisingly, the rate of the shift gets higher under higher pressure. On the other hand, a series of change in absorption ($\Delta\lambda_{max}$) under different pressures is given as a function of logarithmic time scale (Fig. 4c) to provide a simple prediction for the time-pressure superposition. The curve of each pressure in logarithmic time scales allows shifting in the right/left by a constant without a change in the magnitude of $\Delta\lambda_{max}$.

A "time-pressure shift factor" α_P (P) can be defined as a constant that is applied for the horizontal shift of the curve plotted at an arbitrary pressure in order to match it to the curve at a reference pressure. In our case, 40 MPa was particularly assigned as reference curve and α_P is calculated as 0.679, 0.536, and 0.319 min^{-1} for the curves of 160, 120 and 80 MPa, respectively. To obtain a single "master curve" by horizontal shifting, a simple logarithmic calculation is carried out using α_P values of each curve and the negative shift is provided (in arrow direction). In Fig. 4d, the calculated master curve is given as a result of the calculation. Since the curve satisfies

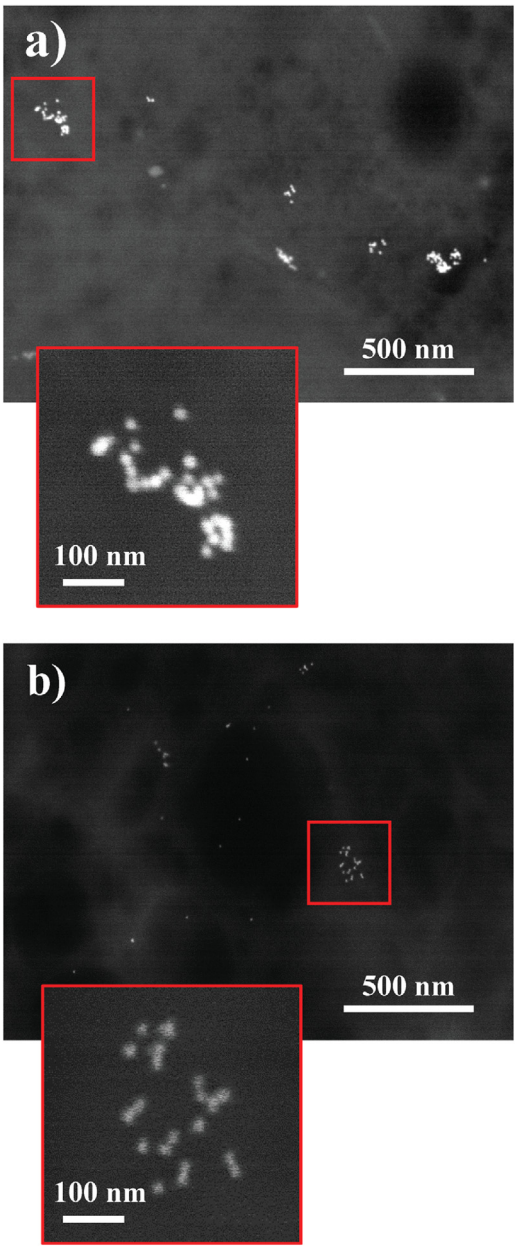

Fig. 3. SEM images of the Au NPs in (a) unloaded and (b) loaded films.

the Boltzmann superposition principle that describes the response of a material to different loading histories, PAAm/Au films have "time-pressure superposition" as a function of shift in absorption [51]. Note that the deformation (creeping) of a linear viscoelastic material follows this mathematical approach. Therefore, the change in absorption may be the evidence for the governing of the color transformation through the rate of deformation and the change in time according to Kelvin-Voigt viscoelastic model.

Since polymer matrix provides a viscous medium for the diffusion during dis/assembly of the Au particles, the viscoelastic properties of the surrounding polymer is a significant parameter for this sensor system. The viscosity of a polymer is exponentially correlated to temperature; therefore one can suggest that a change in temperature causes a dramatic effect on the shift of absorption signal at constant pressure. In this sense, the change in color of PAAm/Au films was investigated in terms of the relation between

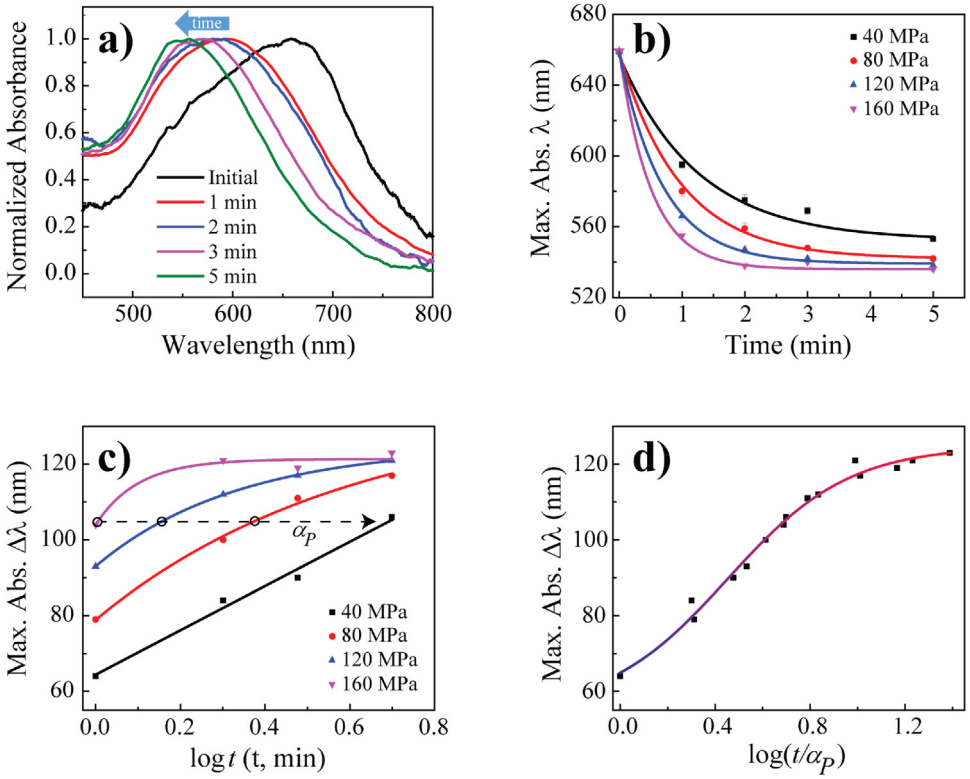

Fig. 4. (a) Absorption spectra of the pressure (40 MPa) applied film for the different duration, (b) the change of the corresponding λ_{max} with respect to time, and (c) $\Delta\lambda_{max}$ in logarithmic time scale for different pressure (shifting factor (αP) is presented with arrow). (d) Time-Pressure superposition of PAAm/Au film.

viscosity and temperature (Eq. 2). The relation can be given according to Exponential Model;

$$\eta(T) = \eta_0 \exp(-bT) \quad (2)$$

where η_0 is absolute viscosity, b is constant, and T is the temperature. In Fig. 5, temperature-dependent minor alterations in absorption signal are given for different pressure scales. At the low pressure of 40 MPa, λ_{max} peak position shifts from 575 nm to 562 nm as the temperature increases to 50 °C. Note that the resolution of spectrometer is 1.02 nm. At constant pressure, viscosity of the composite film is expected to decrease as the temperature increases (according to Eq. 2). Therefore, the rate of deformation increases with the lowered viscosity, and causes the shift of λ_{max} in absorption spectrum to become more dramatic (Fig. 5a). However, for higher-pressure scales, the aforementioned trend in the shift gradually turns into opposite direction and λ_{max} peak starts to increase as the temperature increases (Fig. 5**b** and **c**). This temperature-induced reverse shift may be attributed to a morphological change in the PAAm matrix upon the deformation. In other words, possible crystallization in polymeric structure may have influence on deformation.

To elucidate the morphological changes of the films at elevated temperature, a detailed structural analysis was performed. SEM images and XRD patterns of pressure-loaded and -unloaded films at 50 °C are presented in Fig. 6. The composite film of PAAm matrix and Au NPs shows smooth surface upon compressing with 40 MPa (Fig. 6a). When the pressure is doubled to 80 MPa, the rice-like shape elongated bright structures are surprisingly observed. The diameter of the structures is 305 nm and the length is 960 nm. The shape remains unchanged as rice-like; however, the lengths are getting longer, when the pressure is further increases to 160 MPa. They grow into 480 nm and 2.6 μm, respectively (Fig. 6b and c). These formations consist of a similar chemical structure with the polymer matrix (Fig. S4), therefore the contrast in microscopy images may be attributed to a crystallized polymer structure that are oriented along the flow direction upon application of pressure.

Fig. 6d presents XRD pattern of the PAAm/Au films employed under different deformations at 50 °C. All patterns exhibit characteristic Au signals at 38.9° and 45.1° (2θ), which may belong to (111) and (200) planes, respectively (*JCPDS 04-0784*) [52,53]. The unloaded film shows amorphous halo at initial state, which disappears as the pressure increases. The additional signals that may arise from polymer crystallites are observed at 19.1° and 29.3° (2θ) [54]. The presence of sharp reflections may originate from the occurrence of *pressure-induced crystallization*. Since the polymer chains are packed more closely and tightly in crystalline formation than its amorphous counterpart, the density of crystallites (ρ_c) will be higher than corresponding amorphous region (ρ_a). The ratio of the density of two polymeric morphologies (ρ_c/ρ_a) varies. The mean value of this ratio can be given as 1.13 [55]. For the polymers having both crystalline and amorphous substituents, namely semi-crystalline materials, Eq. 3 gives an approximate relationship between densities of having different crystallinity;

$$\rho_{sc}/\rho_a = 1 + 0.13\chi_c \quad (3)$$

where ρ_{sc} is density of the semi-crystalline polymer and χ_c is the degree of crystallinity. In the case of stress-induced crystallization of PAAm, volumetric loss of equal weighted deformed and non-deformed samples can be defined as difference between volumes of amorphous (V_a) and semi-crystalline (V_{sc}) polymers (Eq. 4). Therefore, the change in peak position with different regimes at elevated temperatures may be attributed to this volumetric loss upon crystallization because it inversely affects the deformation of PAAm/Au film.

$$V_a - V_{sc} = 0.13\chi_c V_{sc} \quad (4)$$

Considering the nature of PAAm, i.e. capability to form hydrogel via H-bonding, it is expected that the pressure sensitive PAAm/Au

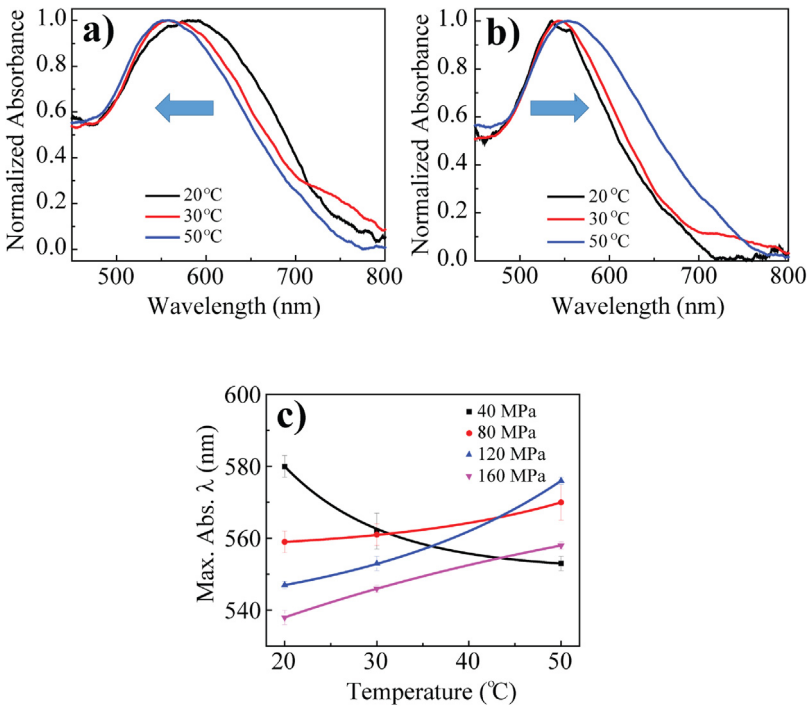

Fig. 5. Absorption spectra of the constant pressure applied films ((a) 40 MPa and (b) 160 MPa) at various temperatures and (c) the change of the corresponding λ_{max} with respect to temperature.

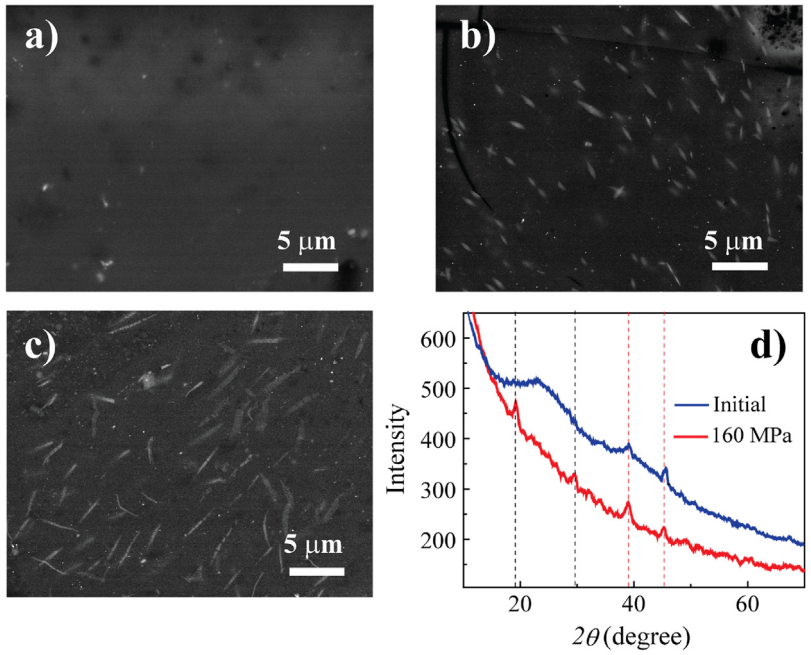

Fig. 6. SEM images of the films in diverse conditions (a) 40 MPa, (b) 80 MPa, and (c)160 MPa at 50 °C (Scale bar: 5 μm), (d) XRD patterns of loaded and unloaded films at 50 °C.

composites can demonstrate structural recovery feature under appropriate conditions to heal cracks, voids, or tears. This feature of the PAAm/Au stimuli-responsive film was determined by dividing the sample into two pieces under ambient condition. The time-evolution of the healing period is presented in Fig. 7 as a photo frame. Initially, the non-deformed bluish films were divided into two pieces and placed 1 mm apart from each other. After a while, it is observed that these two pieces start to contact each other and the gap is completely filled in five days. In general, the self-healing of structures is initiated by an external stimulus such as light, heat, or chemicals that result in the recombination of the primary or secondary bonds [56,57]. Since the acrylamide pendant group consists of acidic-hydrogen, oxygen and nitrogen that are able to form secondary interaction (hydrogen bond) via intermolecules. The recombination of polymer chains may also be triggered by their exposure to water molecules. Not surprisingly, the PAAm matrix in this study having a lower molecular weight (1500 g/mol) is self-recovered by in the presence of moisture in the air.

Considering the cell phones are ubiquitous devices in daily life, smartphone-assisted detection may offer inexpensive and acces-

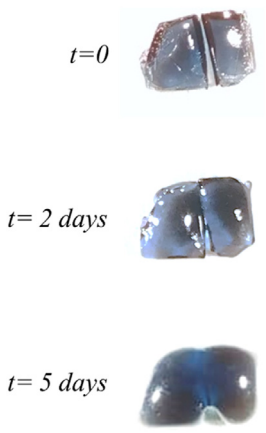

Fig. 7. Photographs of the Au NP/PAAm composite divided into two pieces. The self-healing feature is shown as a function of time.

sible alternative quantifying dramatic color change of PAAm/Au films [58]. In this sense, since almost all the cell phones have the ability to take a photograph today, a simple algorithm in order to estimate applied pressure is proposed here as a possible cell phone application. Under a fixed pressure, a PAAm/Au composite film can response a particular color back from a range spanning a continuous color distribution between blue and red. Even though data points regarding to color versus applied pressure have been obtained throughout this study are discrete (because there are only 5 data in total representing the color vs pressure from 0 to 160 MPa), one can try to search for a possible pattern that these data points may follow in order to obtain a continuous one-to-one matching of color-pressure distribution. By using such a pattern, one can design a regression algorithm based on performing image processing on the taken photograph of PAAm/Au composite film to estimate the applied pressure even apart from the ones used in this study. Captured photograph of any sample shows variation in the red and blue color values obtained from RGB space of the corresponding pixels depending on the parameters such as distance, illumination, background light, and angle between the phone and sample. However, for simulation of user behavior, corresponding photographs were captured randomly by using cell phone under daylight without concerning any of the aforementioned parameters in detail. To reduce estimation error, a satisfactory dataset should be constructed to improve the training pattern, which can be achieved by employing multiple images (more photos should be captured randomly) at each corresponding pressure. In this sense, dataset consists of two different sample set consisting of initial state and 40, 80, 120, and 160 MPa pressures, and their three different photographs were considered. To train algorithm, for every pressure including initial state, there are five of different corresponding images were employed. This training dataset, as presented in Fig. 8, was then used to determine average red (red plot) and blue (blue plot) pixel values of every image referring to its corresponding pressure. As the pressure increases, corresponding average pixel values for red follow an increasing linear curve while blue follows a decreasing linear pattern as expected. To reduce the dimension in order to simplify the algorithm, the ratio of these two parameters (red/blue) was considered. Red/blue coordinates versus applied pressure fit to almost a perfect linear curve, which hints about that there is a significant error reduction compared to case of analyzing red and blue individually. Remaining sample (Sample 6) was employed as test dataset to estimate pressure and calculate corresponding errors. As illustration, the image of the resulting color under 80 MPa pressure was considered. After taking its photograph by cell phone through application, algorithm behind this application calculates the red/blue immediately, which was found as 1.15 for this case. Then, by putting 1.15 as y in linear equation of $y = mx + b$, where m (0.00494), and b (0.74501) already determined through curve fitting process, one can obtain the corresponding pressure as x. Here, pressure was calculated as 81.9 MPa, which has an error ≅2%. For the remaining samples, from 0 to 160 MPa, estimated pressures and their errors were given in **Table S2**. For the further reduction of error, one can produce and use more samples in training dataset or optimize the image processing techniques since cropping the interested region from the rest of the image leads to information loss while determining the values of red and blue. Nevertheless, algorithm proposed in this study has sufficient error rates, it is sim-

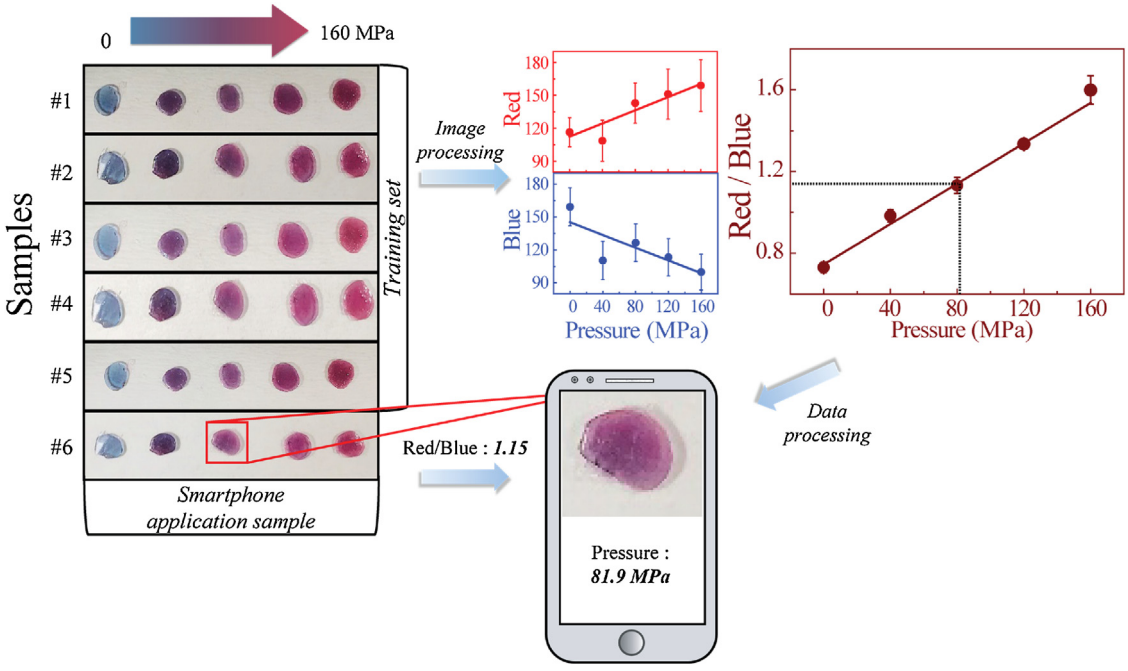

Fig. 8. Schematic illustration of smart-phone application and linear curve of red and blue color intensity.

ple, and can be employed as cell phone application to estimate the pressure using the resulting color of PAAm/Au composite.

4. Conclusions

A stress-responsive colorimetric PAAm/Au films having self-healing properties were fabricated and their optical response upon external mechanical force was examined. Initially, the films with dark blue color turn into ruby red as the 160 MPa of pressure is applied due to the disassembly of Au NP clusters in the film. Since PAAm chains laterally flow under the pressure, the motion of polymer acts as a part of the disassembly during a deformation. The distinct plasmonic shift is strongly correlated to mechanical properties of the surrounding matrix. Therefore, the colorimetric response depends not only on the magnitude of applied pressure but also its duration. Therefore, the stimuli-responsive PAAm/Au films can be employed even lower pressure scales by extending the duration of applied pressure. A further shift in absorbance was observed at lower pressures as the temperature increases probably due to decreasing the viscosity of PAAm. Moreover, for the practical applicability of the PAAm/Au films, RGB space-based algorithm was developed to use in a simple smart-phone application for photographic detection of applied pressure with ≅2% error. The ease of chemical modification and biocompatibility of PAAm matrix may allow developing a wide variety of Au-based colorimetric pressure sensors.

Associated content

Supporting Information includes zeta potential of Au NPs, Energy Dispersive X-ray spectra of PAAm crystallites, DSC curve and absorption spectra of the films, and dataset for RGB algorithm.

Acknowledgement

The authors gratefully acknowledge funding from The Scientific and Technological Research Council of Turkey (TUBITAK, 1001 117Z331).

Appendix A. Supplementary data

Supplementary material related to this article can be found, in the online version, at doi:https://doi.org/10.1016/j.sna.2019.06.038.

References

[1] D.J. Lipomi, M. Vosgueritchian, B.C. Tee, S.L. Hellstrom, J.A. Lee, C.H. Fox, Z. Bao, Skin-like pressure and strain sensors based on transparent elastic films of carbon nanotubes, Nat. Nanotechnol. 6 (2011) 788.
[2] C. Wang, D. Hwang, Z. Yu, K. Takei, J. Park, T. Chen, B. Ma, A. Javey, User-interactive electronic skin for instantaneous pressure visualization, Nat. Mater. 12 (2013) 899.
[3] G. Schwartz, B.C.-K. Tee, J. Mei, A.L. Appleton, D.H. Kim, H. Wang, Z. Bao, Flexible polymer transistors with high pressure sensitivity for application in electronic skin and health monitoring, Nat. Commun. 4 (2013) 1859.
[4] L. Viry, A. Levi, M. Totaro, A. Mondini, V. Mattoli, B. Mazzolai, L. Beccai, Flexible three-axial force sensor for soft and highly sensitive artificial touch, Adv. Mater. 26 (2014) 2659–2664.
[5] M. Cheng, X. Huang, C. Ma, Y. Yang, A flexible capacitive tactile sensing array with floating electrodes, J. Micromech. Microeng. 19 (2009) 115001.
[6] Q. Gao, H. Meguro, S. Okamoto, M. Kimura, Flexible tactile sensor using the reversible deformation of poly (3-hexylthiophene) nanofiber assemblies, Langmuir 28 (2012) 17593–17596.
[7] D. Mandal, S. Yoon, K.J. Kim, Origin of piezoelectricity in an electrospun poly (vinylidene fluoride-trifluoroethylene) nanofiber web-based nanogenerator and nano-pressure sensor, Macromol. Rapid Comm. 32 (2011) 831–837.
[8] D.J. Cohen, D. Mitra, K. Peterson, M.M. Maharbiz, A highly elastic, capacitive strain gauge based on percolating nanotube networks, Nano Lett. 12 (2012) 1821–1825.
[9] Y. Yang, H. Zhang, Z.-H. Lin, Y.S. Zhou, Q. Jing, Y. Su, J. Yang, J. Chen, C. Hu, Z.L. Wang, Human skin based triboelectric nanogenerators for harvesting biomechanical energy and as self-powered active tactile sensor system, ACS Nano 7 (2013) 9213–9222.
[10] C. Pang, G.-Y. Lee, T.-i. Kim, S.M. Kim, H.N. Kim, S.-H. Ahn, K.-Y. Suh, A flexible and highly sensitive strain-gauge sensor using reversible interlocking of nanofibres, Nat. Mater. 11 (2012) 795.
[11] L. Lin, Y. Xie, S. Wang, W. Wu, S. Niu, X. Wen, Z.L. Wang, Triboelectric active sensor array for self-powered static and dynamic pressure detection and tactile imaging, ACS Nano 7 (2013) 8266–8274.
[12] M. Segev-Bar, A. Landman, M. Nir-Shapira, G. Shuster, H. Haick, Tunable touch sensor and combined sensing platform: toward nanoparticle-based electronic skin, ACS Appl. Mater. Inter. 5 (2013) 5531–5541.
[13] T. Yamada, Y. Hayamizu, Y. Yamamoto, Y. Yomogida, A. Izadi-Najafabadi, D.N. Futaba, K. Hata, A stretchable carbon nanotube strain sensor for human-motion detection, Nat. Nanotechnol. 6 (2011) 296.
[14] G.H. Lee, T.M. Choi, B. Kim, S.H. Han, J.M. Lee, S.-H. Kim, Chameleon-inspired mechanochromic photonic films composed of non-close-Packed colloidal arrays, ACS Nano 11 (2017) 11350–11357.
[15] T. Ito, C. Katsura, H. Sugimoto, E. Nakanishi, K. Inomata, Strain-responsive structural colored elastomers by fixing colloidal crystal assembly, Langmuir 29 (2013) 13951–13957.
[16] X. Han, Y. Liu, Y. Yin, Colorimetric stress memory sensor based on disassembly of gold nanoparticle chains, Nano Lett. 14 (2014) 2466–2470.
[17] Z.Z. Gu, H. Uetsuka, K. Takahashi, R. Nakajima, H. Onishi, A. Fujishima, O. Sato, Structural color and the lotus effect, Angew. Chemie Int. Ed. English 42 (2003) 894–897.
[18] G. Topçu, T. Güner, M.M. Demir, Non-iridescent structural colors from uniform-sized SiO 2 colloids, Photonics Nanostruct. 29 (2018) 22–29.
[19] A. Vanderkooy, Y. Chen, F. Gonzaga, M.A. Brook, Silica shell/gold core nanoparticles: correlating shell thickness with the plasmonic red shift upon aggregation, ACS Appl. Mater. Inter. 3 (2011) 3942–3947.
[20] D. Ge, E. Lee, L. Yang, Y. Cho, M. Li, D.S. Gianola, S. Yang, A robust smart window: reversibly switching from high transparency to angle-independent structural color display, Adv. Mater. 27 (2015) 2489–2495.
[21] A. Rankin, S. McGarry, A flexible pressure sensitive colour changing device using plasmonic nanoparticles, Nanotechnology 26 (2015) 075502.
[22] N. Jiang, X. Zhuo, J. Wang, Active plasmonics: principles, structures, and applications, Chem. Rev. 118 (2017) 3054–3099.
[23] K. Saha, S.S. Agasti, C. Kim, X. Li, V.M. Rotello, Gold nanoparticles in chemical and biological sensing, Chem. Rev. 112 (2012) 2739–2779.
[24] S. Zeng, K.-T. Yong, I. Roy, X.-Q. Dinh, X. Yu, F. Luan, A review on functionalized gold nanoparticles for biosensing applications, Plasmonics 6 (2011) 491.
[25] Z. Qian, D.S. Ginger, Reversibly reconfigurable colloidal plasmonic nanomaterials, J. Am. Chem. Soc. 139 (2017) 5266–5276.
[26] Y. Zhao, L. Cao, J. Ouyang, M. Wang, K. Wang, X.-H. Xia, Reversible plasmonic probe sensitive for pH in micro/nanospaces based on i-motif-modulated morpholino-gold nanoparticle assembly, Anal. Chem. 85 (2012) 1053–1057.
[27] S.E. Lee, Q. Chen, R. Bhat, S. Petkiewicz, J.M. Smith, V.E. Ferry, A.L. Correia, A.P. Alivisatos, M.J. Bissell, Reversible aptamer-Au plasmon rulers for secreted single molecules, Nano Lett. 15 (2015) 4564–4570.
[28] Y. Yan, S. Samai, K.L. Bischoff, J. Zhang, D.S. Ginger, Photocontrolled DNA hybridization stringency with fluorescence detection in heterogeneous assays, ACS Sens. 1 (2016) 566–571.
[29] J. Zhang, X. Xu, C. Yang, F. Yang, X. Yang, Colorimetric iodide recognition and sensing by citrate-stabilized core/shell Cu@ Au nanoparticles, Anal. Chem. 83 (2011) 3911–3917.
[30] W. Zhao, W. Jia, M. Sun, X. Liu, Q. Zhang, C. Zong, J. Qu, H. Gai, Colorimetric detection of Cu2+ by surface coordination complexes of polyethyleneimine-capped Au nanoparticles, Sensor. Actuat. B-Chem. 223 (2016) 411–416.
[31] Y. Cho, S.S. Lee, J.H. Jung, Recyclable fluorimetric and colorimetric mercury-specific sensor using porphyrin-functionalized Au@ SiO 2 core/shell nanoparticles, Analyst 135 (2010) 1551–1555.
[32] D. Wen, W. Liu, A.K. Herrmann, D. Haubold, M. Holzschuh, F. Simon, A. Eychmüller, Simple and sensitive colorimetric detection of dopamine based on assembly of cyclodextrin-modified Au nanoparticles, Small 12 (2016) 2439–2442.
[33] S. Chah, M.R. Hammond, R.N. Zare, Gold nanoparticles as a colorimetric sensor for protein conformational changes, Chem. Bio. 12 (2005) 323–328.
[34] C. Wang, Y. Du, Q. Wu, S. Xuan, J. Zhou, J. Song, F. Shao, H. Duan, Stimuli-responsive plasmonic core–satellite assemblies: i-motif DNA linker enabled intracellular pH sensing, Chem. Commun. 49 (2013) 5739–5741.
[35] S. Sun, X. Ning, G. Zhang, Y.C. Wang, C. Peng, J. Zheng, Dimerization of organic dyes on luminescent gold nanoparticles for ratiometric pH sensing, Angew. Chemie Int. Ed. English 55 (2016) 2421–2424.
[36] X.-Y. Liu, F. Cheng, Y. Liu, W.-G. Li, Y. Chen, H. Pan, H.-J. Liu, Thermoresponsive gold nanoparticles with adjustable lower critical solution temperature as colorimetric sensors for temperature, pH and salt concentration, J. Mater. Chem. 20 (2010) 278–284.
[37] M. Tagliazucchi, M.G. Blaber, G.C. Schatz, E.A. Weiss, I. Szleifer, Optical properties of responsive hybrid Au@ polymer nanoparticles, ACS Nano 6 (2012) 8397–8406.
[38] Y. Liu, X. Han, L. He, Y. Yin, Thermoresponsive assembly of charged gold nanoparticles and their reversible tuning of plasmon coupling, Angew. Chemie Int. Ed. English 51 (2012) 6373–6377.

[39] J.I. Chen, Y. Chen, D.S. Ginger, Plasmonic nanoparticle dimers for optical sensing of DNA in complex media, J. Am. Chem. Soc. 132 (2010) 9600–9601.
[40] G.K. Joshi, K.N. Blodgett, B.B. Muhoberac, M.A. Johnson, K.A. Smith, R. Sardar, Ultrasensitive photoreversible molecular sensors of azobenzene-functionalized plasmonic nanoantennas, Nano Lett. 14 (2014) 532–540.
[41] Y. Yan, J.I. Chen, D.S. Ginger, Photoswitchable oligonucleotide-modified gold nanoparticles: controlling hybridization stringency with photon dose, Nano Lett. 12 (2012) 2530–2536.
[42] F. Huang, J.J. Baumberg, Actively tuned plasmons on elastomerically driven Au nanoparticle dimers, Nano Lett. 10 (2010) 1787–1792.
[43] A.C. Balazs, T. Emrick, T.P. Russell, Nanoparticle polymer composites: where two small worlds meet, Science 314 (2006) 1107–1110.
[44] K. Spildo, E.I.Ø. Sæ, Effect of charge distribution on the viscosity and viscoelastic properties of partially hydrolyzed polyacrylamide, Energ. Fuel. 29 (2015) 5609–5617.
[45] J.C. Munro, C.W. Frank, Polyacrylamide adsorption from aqueous solutions on gold and silver surfaces monitored by the Quartz Crystal Microbalance, Macromolecules 37 (2004) 925–938.
[46] J. Bai, Y. Li, J. Du, S. Wang, J. Zheng, Q. Yang, X. Chen, One-pot synthesis of polyacrylamide-gold nanocomposite, Mater. Chem. Phys. 106 (2007) 412–415.
[47] M.C. Darnell, J.-Y. Sun, M. Mehta, C. Johnson, P.R. Arany, Z. Suo, D.J. Mooney, Performance and biocompatibility of extremely tough alginate/polyacrylamide hydrogels, Biomaterials 34 (2013) 8042–8048.
[48] J. Turkevich, P.C. Stevenson, J. Hillier, A study of the nucleation and growth processes in the synthesis of colloidal gold, Discuss. Faraday Soc. 11 (1951) 55–75.
[49] Z. Zhong, S. Patskovskyy, P. Bouvrette, J.H.T. Luong, A. Gedanken, The surface chemistry of Au colloids and their interactions with functional amino acids, J. Phys. Chem. B 108 (2004) 4046–4052.
[50] T. Ung, L.M. Liz-Marzán, P. Mulvaney, Optical properties of thin films of Au@SiO2 particles, J. Phys. Chem. B 105 (2001) 3441–3452.
[51] D. Roylance, Engineering viscoelasticity, vol. 2139, Department of Materials Science and Engineering–Massachusetts Institute of Technology, Cambridge MA, 2001, pp. 1–37.
[52] D. Philip, Biosynthesis of Au, Ag and Au–Ag nanoparticles using edible mushroom extract, Spectrochim. Acta A. 73 (2009) 374–381.
[53] C. Shen, C. Hui, T. Yang, C. Xiao, J. Tian, L. Bao, S. Chen, H. Ding, H. Gao, Monodisperse noble-metal nanoparticles and their surface enhanced Raman scattering properties, Chem. Mater. 20 (2008) 6939–6944.
[54] F. Yan, C. Zheng, X. Zhai, D. Zhao, Preparation and characterization of polyacrylamide in cationic microemulsion, J. Appl. Polym. Sci. 67 (1998) 747–754.
[55] D.W. Van Krevelen, K. Te Nijenhuis, Properties of Polymers: Their Correlation With Chemical Structure; Their Numerical Estimation and Prediction From Additive Group Contributions, Elsevier, 2009.
[56] G. Wypych, Self-Healing Materials: Principles and Technology, Elsevier, 2017.
[57] W.H. Binder, Self-healing Polymers: From Principles to Applications, John Wiley & Sons, 2013.
[58] A. İncel, O. Akın, A. Çağır, Ü.H. Yıldız, M.M. Demir, Smart phone assisted detection and quantification of cyanide in drinking water by paper based sensing platform, Sens. Actuators B-Chem. 252 (2017) 886–893.

Biographies

Gokhan Topcu received his BSc in Chemistry (2013) and MSc in Organic Chemistry (2015) from the Marmara University, respectively. He has been carrying out his doctoral research on advanced polymeric composites and nanomaterials at Department of Materials Science and Engineering in İzmir Institute of Technology since 2015. His current researches are on the development of mechanical sensors by using plasmonic and photonic nanostructures in polymeric systems.

Tugrul Guner received his BSc in Physics (2011) from Bilkent University, MSc in Physics (2015) from Izmir Institute of Technology, and PhD in Materials Science and Engineering (2018) from Izmir Institute of Technology. He studied down-converting materials and their white light applications during his doctoral thesis. He is currently postdoctoral fellow in Centre Énergie Matériaux Télécommunications (EMT) at Institut National de la Recherche Scientifique (INRS) in Quebec (Canada), and he is currently conducting researches on understanding and imaging of the ultrafast dynamics of nanomaterials using ultrafast transmission electron microscopy.

Ezgi Inci received her BSc in Material Science and Engineering (2017) from the Anadolu University. She has been carrying out her MSc on inorganic nanomaterials and polymeric composites at Department of Materials Science and Engineering in İzmir Institute of Technology since 2017. Her current research is based on the fabrication of Langmuir Blodgett coatings and mechanical sensors.

Mustafa M. Demir is Professor at the Izmir Institute of Technology, Department of Materials Science and Engineering. He coordinates an interdisciplinary group working on synthesis and nanotechnologies on soft matter. His research activity is focused on the development of polymeric optical nanocomposites for advanced applications, electrospinning, and functional systems. He has been awarded the "Young researcher" Prize of Turkish Academy of Sciences in 2013. His details can be found at: http://www.demirlab.iyte.edu.tr.